Barrier transmission for proton emission during the intranuclear cascade process

Yuji Yamaguchi* and Yusuke Uozumi
Department of Applied Quantum Physics and Nuclear Engineering, Kyushu University, 744 Motooka, Nishi-ku, Fukuoka 819-0395, Japan

Masahiro Nakano
Junshin Gakuen University, 1-1-1 Chikushigaoka, Minami-ku, Fukuoka 815-8510, Japan

(Received 9 April 2019; published 23 September 2019)

A method is proposed for determining the barrier transmission coefficient for the outgoing protons from the intranuclear cascade process in $(p,\ p'x)$ reactions. In this method, the coefficient is defined as the ratio of the cross section of the proton-nucleus reaction to that of the neutron-nucleus reaction and is calculated by using empirical equations for the cross sections with no free parameters. The determined coefficient is incorporated into an intranuclear cascade model followed by an evaporation model, and the double-differential cross sections are calculated for $(p,\ p'x)$ reactions around 50 MeV on heavy targets with $A \geqslant 120$. The present results agree well with experimental observations. Remarkably, the spectra for ^{209}Bi and ^{197}Au are accounted for even though the evaporation contributions are negligibly small.

DOI: 10.1103/PhysRevC.100.034617

I. INTRODUCTION

The continuum of $(p,\ p'x)$ reactions has been investigated with various theoretical models, including the intranuclear cascade (INC) model [1] and the quantum molecular dynamics model [2]. Although outgoing protons from the cascade process must penetrate the barriers presented by the Coulomb and centrifugal potentials, little attention has been paid to the barrier transmission. In a recent paper [3], the barrier transmission coefficient $P_{\rm tr}$ was introduced into the INC model, and its important contribution was revealed in $(p,\ p'x)$ reactions in the 50-MeV region.

The basis for applying the INC model to energies below 200 MeV has been controversial, especially the assumption of localized collisions between two particles. One consideration [4] is that this assumption may lose its validity because of the longer wavelengths in the low-energy range. Another is the opposite claim [5,6] that a long wavelength causes interference between scattered waves arising from different positions; however, in continuum excitations scattered waves are canceled out, and consequently the local-collision assumption holds. Recent papers on the INC model [3,7] have shown that if additional physics—namely, the deflection of the particle trajectory, the collective excitations of the target nucleus, and the barrier transmission of outgoing particles—is properly included, then the INC model accounts well for observed double-differential cross-section (DDX) spectra. More recently, the importance of these factors was shown for $(p,\ dx)$ reactions [8] and α-breakup reactions [9]; the importance of these physics is explained explicitly in Ref. [3].

In Ref. [3], the deflection and collective excitations are parameterized using various experimental data on proton-nucleus elastic scattering and exclusive $(p,\ p')$ transitions to collective excitations, respectively, and then incorporated in the INC model. Consequently, their uncertainties are viewed as being relatively low. By contrast, $P_{\rm tr}$ is determined differently: A function is introduced in the form of a Wentzel-Kramers-Brillouin (WKB) solution, and its parameters are adjusted to provide the best match with experimental $(p,\ p'x)$ spectra. However, because the experiments involve not only the cascade process but also the evaporation process, the determined parameters involve uncertainties. Although it is true that the calculations have succeeded in explaining various experimental observations, small overestimations remain in a narrow part of the spectra for heavy targets with $A \geqslant 120$. Consequently, a deeper understanding of the barrier transmission phenomenon is indispensable for developing a more sophisticated method to determine $P_{\rm tr}$ with lower uncertainty.

Regarding the evaporation process, $P_{\rm tr}$ is frequently obtained with the one-dimensional Coulomb potential [10] in terms of the WKB approximation. The alternative is to use optical-model potentials in the calculation, but the resultant values are known to require serious modification [11–15] for a reasonable fit with experiments. It has also reported that the obtained values can be expressed by a Hill-Wheeler-type function or the Fermi function [16], but these functions appear to be unsuitable for the cascade process [3]. Regarding the centrifugal barrier, there is no appropriate way to determine $P_{\rm tr}$. Because the system with which we are concerned reaches a scale of at most $l \approx 10\,\hbar$, the WKB approximation is not applicable.

In this paper, we limit our consideration to $(p,\ p'x)$ reactions in the 50-MeV region, where $P_{\rm tr}$ plays an important role, and we propose a new method for determining $P_{\rm tr}$ in $(p,\ p'x)$

*yyamaguchi@nucl.kyushu-u.ac.jp

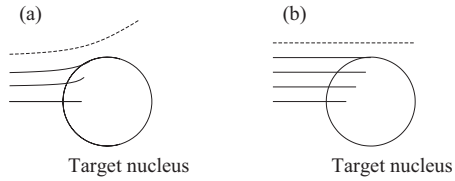

FIG. 1. Classical trajectories for incident (a) protons and (b) neutrons.

reactions that uses proton-nucleus and neutron-nucleus reaction cross sections. We apply the determined coefficient to INC calculations and validate the model by comparing it with experimental observations for heavy target nuclei with $A \geqslant 120$. In the case of light- and medium-weight nuclei, the effect of the barrier transmission is not observed [3] because of the strong contribution of evaporated protons from nuclear equilibrium states.

II. MODEL

A. INC model

The INC model used in this work is described in detail in Ref. [3], and only its essential aspects are described herein. In the basic INC model, energy is transferred to the target nucleus by a sequential *NN* collision only. The initial nucleon positions in the spherical target nucleus are given randomly. The nucleon density follows a Woods-Saxon distribution for a nucleus with radius $r_0 = (0.976 + 0.0206A^{1/3})A^{1/3}$ fm and diffuseness $a_0 = 0.54$ fm. The maximum radius is defined as $R_{\max} = r_0 + 4a_0$. The nucleons in the nucleus are confined in a square-well potential of depth $V_0 = -45$ MeV, and the initial momenta of the nucleons are distributed uniformly in a Fermi sphere. After the initial state is given, an incident proton with an impact parameter b given at random enters the target nucleus and can induce sequential *NN* collisions. If two nucleons i and j become closer than the *NN* cross section σ_{NN}, that is,

$$r_{ij} < \sqrt{\frac{\sigma_{NN}}{\pi}}, \tag{1}$$

then they can collide. The occurrence of the collision is judged using a Pauli blocking operator,

$$\hat{Q}|ij\rangle = \Theta(E_i - E_F)\Theta(E_j - E_F)|ij\rangle, \tag{2}$$

where E_i is the kinetic energy of nucleon i after the collision, E_F is the Fermi energy, and Θ is the unit step function.

In the extended INC model used herein, additional physical processes are included to describe the medium-energy reactions involved in the deflection of particle trajectory, the collective excitations of the target nucleus, and the barrier transmission of the outgoing particles. Therefore, the proton emission probability $P^{(p)}$ as a function of the outgoing proton kinetic energy ε and emission angle θ is written as

$$P^{(p)}(\theta,\varepsilon) = P^{(p)}_{\rm def}(1+P_{\rm CE})[\hat{G} + \hat{G}(\hat{Q}P_{NN})\hat{G} + \hat{G}(\hat{Q}P_{NN})\hat{G}(\hat{Q}P_{NN})\hat{G} + \cdots]P^{(p)}_{\rm tr}P^{(p)}_{\rm def}|_{\theta,\varepsilon}, \tag{3}$$

where the processes are arranged from left to right, and $P^{(p)}_{\rm def}$, $P_{\rm CE}$, and $P^{(p)}_{\rm tr}$ are the probabilities of proton deflection, collective excitation, and barrier transmission for the escaping

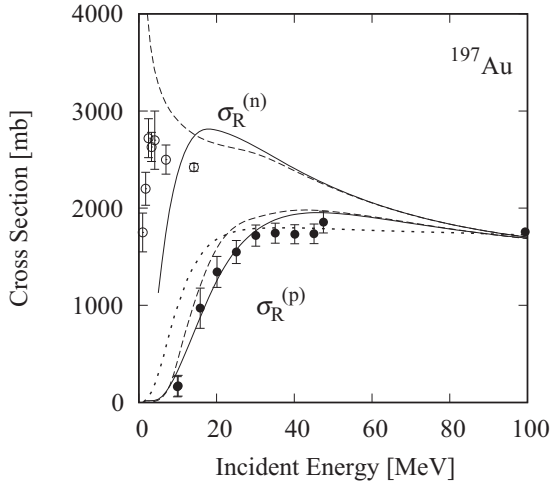

FIG. 2. Experimental and calculated neutron-nucleus and proton-nucleus reaction cross sections for a ^{197}Au target. Experimental values of $\sigma_R^{(n)}$ and $\sigma_R^{(p)}$ are shown by open and closed circles, respectively. Curves show calculation results from empirical formulas (see text for details).

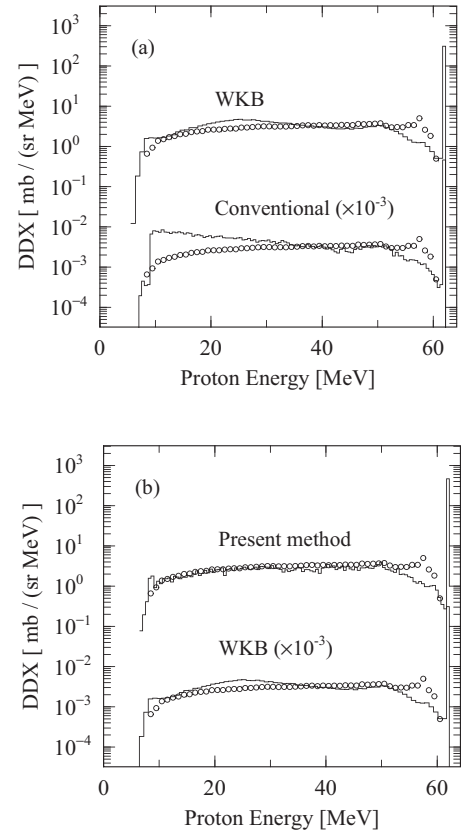

FIG. 3. ^{209}Bi(p, $p'x$) spectra at 30° for $E_p = 61.7$ MeV. Results calculated with different transmission coefficients are compared. See text for full details.

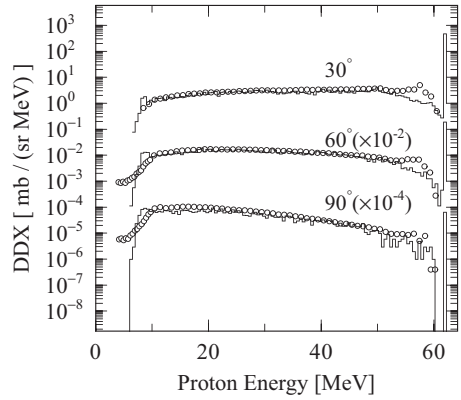

FIG. 4. ^{209}Bi$(p,\ p'x)$ spectra for $E_p = 61.7$ MeV. Circles, experimental data; solid lines, calculation results.

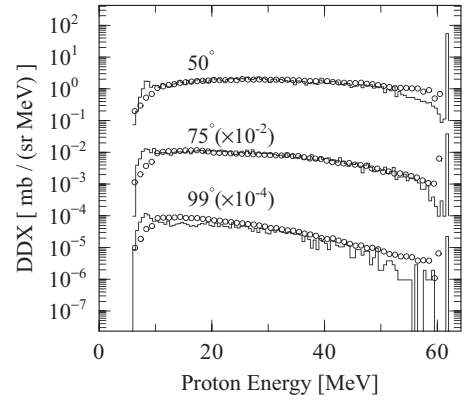

FIG. 6. ^{197}Au$(p,\ p'x)$ spectra for $E_p = 61.5$ MeV. Circles, experimental data; solid lines, calculation results.

proton, respectively. The operator $\hat{G}$ expresses the spatial development of energetic particles, which travel in straight lines inside the nucleus, and P_{NN} is the NN collision probability to fulfill Eq. (1). Finally, the DDX for the $(p,\ p'x)$ reaction is calculated by

$$\left.\frac{d^2\sigma}{dEd\Omega}\right|_{\theta,\varepsilon} = \sigma_{\text{total}}\frac{1}{2\pi\Delta E\Delta\cos\theta}P^{(p)}(\theta,\varepsilon), \tag{4}$$

where ΔE and $\Delta\cos\theta$ are the bin widths of the outgoing energy ε and emission angle θ, respectively, and $\sigma_{\text{total}} = \pi R^2_{\text{max}}$ is the proton-nucleus total cross section.

B. Barrier transmission coefficient

To investigate the barrier transmission coefficient for outgoing particles, we consider that for the inverse process, namely, incident particles. Figures 1(a) and 1(b) show the classical trajectories for protons and neutrons, respectively, impinging on the target nucleus. The entrance window for protons clearly has a smaller area than that for neutrons, and thus the reaction cross section for protons is smaller than that for neutrons. This is due to the effect of the Coulomb potential on incoming protons.

The cross section for neutron-nucleus reactions can be approximated by

$$\sigma_{\text{R}}^{(n)} = \pi b^2_{\text{max}} P_{\text{tr}}^{(n)} P_{nN}, \tag{5}$$

where $P_{\text{tr}}^{(n)}$ is the barrier transmission coefficient of neutrons penetrating the barrier presented by the centrifugal potential, and P_{nN} is the probability of neutron-nucleon interactions inside the nucleus. The parameter b_{max} is the maximum impact parameter. If b_{max} for neutron incidence is the maximum nuclear radius R_{max}, then $P_{\text{tr}}^{(n)}$ is expressed by

$$P_{\text{tr}}^{(n)} = \begin{cases} 1 & : b \leqslant b_{\text{max}} \\ 0 & : b > b_{\text{max}}. \end{cases} \tag{6}$$

Similarly, the proton-nucleus reaction cross section is written as

$$\sigma_{\text{R}}^{(p)} = \pi b^2_{\text{max}} P_{\text{tr}}^{(p)} P_{pN}, \tag{7}$$

where all the parameters are as those in Eq. (5) but for protons. The transmission coefficient $P_{\text{tr}}^{(p)}$ gives the proton transmission probability for the barrier presented by the centrifugal and Coulomb potentials. Figure 1(a) implies that $P_{\text{tr}}^{(p)}$ should be a function whose value changes gradually with the impact parameter. Assuming charge symmetry, we obtain the

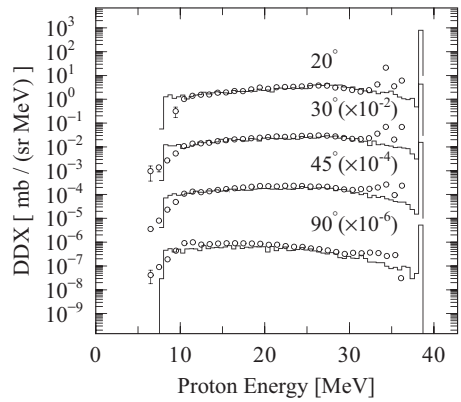

FIG. 5. ^{209}Bi$(p,\ p'x)$ spectra for $E_p = 38.7$ MeV. Circles, experimental data; solid lines, calculation results.

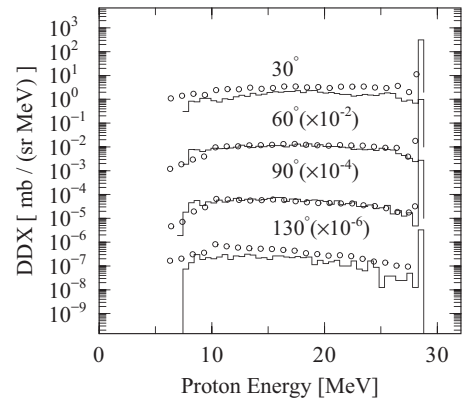

FIG. 7. ^{197}Au$(p,\ p'x)$ spectra for $E_p = 28.8$ MeV. Circles, experimental data; solid lines, calculation results.

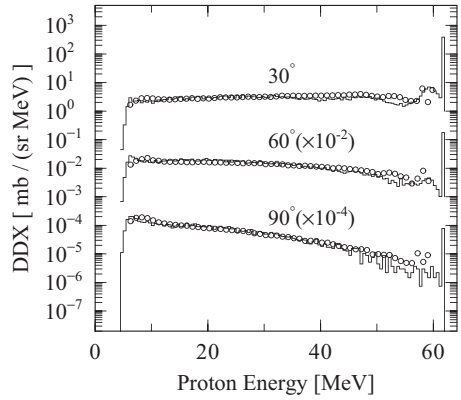

FIG. 8. ^{120}Sn$(p,\ p'x)$ spectra for $E_p = 61.5$ MeV. Circles, experimental data; solid lines, calculation results.

relationship

$$P_{nN} \approx P_{pN}. \tag{8}$$

From the above discussion, we obtain

$$P_{\rm tr}^{(p)} = \frac{\sigma_{\rm R}^{(p)}}{\sigma_{\rm R}^{(n)}}. \tag{9}$$

The emitted particles travel along the same trajectories as the solid lines in Fig. 1, but in the opposite direction. Therefore, the exit window for protons must be smaller than that for neutrons, and the flux of escaping protons is suppressed because of the potential by the factor given by Eq. (9).

As for $\sigma_{\rm R}^{(n)}$ and $\sigma_{\rm R}^{(p)}$, many efforts were made before the 1980s to measure their values. However, the experimental errors were large, and there was a severe lack of data with respect to energy and targets. Therefore, we must turn to empirical formulas, some of which are used for comparison in Fig. 2. In this figure, the experimental values of the neutron-nucleus reaction cross section (open circles) and the proton-nucleus reaction cross section (closed circles) for ^{197}Au are taken from the EXFOR library of experimental nuclear reaction data [17]. Calculations of $\sigma_{\rm R}^{(n)}$ are shown for the Pearlstein formula [18] by a solid line and the Pearlstein-Niita formula

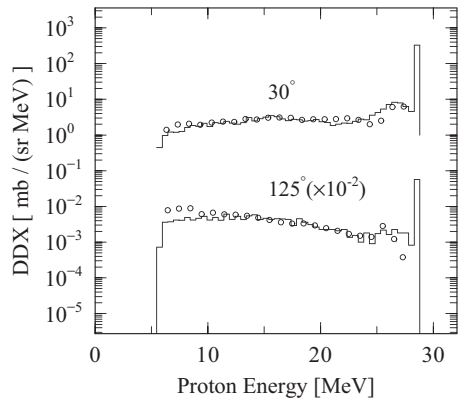

FIG. 9. ^{120}Sn$(p,\ p'x)$ spectra for $E_p = 28.8$ MeV. Circles, experimental data; solid lines, calculation results.

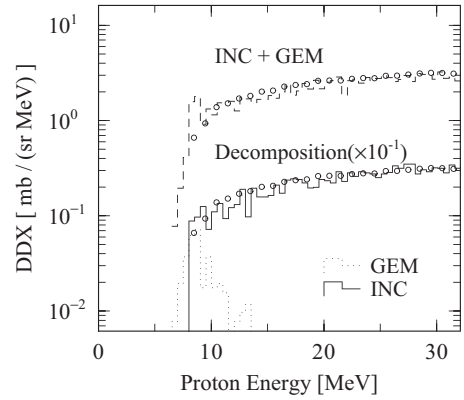

FIG. 10. ^{209}Bi$(p,\ p'x)$ spectra at 30° for $E_p = 61.7$ MeV. The upper part of the figure is the comparison with the sum of INC and GEM. The lower part of the figure shows the comparison with each decomposed component, namely INC (solid line) and GEM (dotted line).

[19] by a dashed line. Calculations of $\sigma_{\rm R}^{(p)}$ are shown for the Shen formula [20] by a solid line, the Pearlstein-Niita formula by a dashed line, and the Wellisch-Axen formula [21] by a dotted line. From these results, we use the systematic formulas of Pearlstein for the neutron-nucleus reaction cross section:

$$\begin{aligned} \sigma_{\rm R}^{(n)} &= 0.045A^{0.7} f^{(n)}(A) g^{(n)}(E), \\ f^{(n)}(A) &= 1 + 0.016\sin(5.3 - 2.63\ln A), \\ g^{(n)}(E) &= 1 - 0.62e^{-\frac{E}{200}}\sin(10.9E^{-0.28}), \end{aligned} \tag{10}$$

and those of Shen for the proton-nucleus reaction cross section, namely,

$$\begin{aligned} \sigma_{\rm R}^{(p)} &= 0.0426A^{0.701} f^{(p)}(A) g^{(p)}(E) h(A,E), \\ f^{(p)}(A) &= 1 + 0.0144\sin(3.63 - 2.82\ln A), \\ g^{(p)}(E) &= 1 - 0.67e^{-\frac{E}{150}}\sin(12E^{-0.289}), \\ h(A,E) &= [1 + (0.018A^2 - 1.15A)E^{-2}]^{-1}, \end{aligned} \tag{11}$$

where A is the target mass and E is the incident energy. The cross sections and the incident energy are expressed in units of barns and mega-electron volts, respectively.

III. RESULTS AND DISCUSSION

To validate the present model, we calculated DDX spectra for $(p,\ p'x)$ reactions using the proposed model followed by the generalized evaporation model (GEM) [22]. The threshold energy for an outgoing proton from a nucleus with charge Z is defined as $kZe^2/(1.7A^{1/3})$ in the GEM, and the same was used in the INC calculations. In Figs. 3–9, the calculated results are compared with experimental data obtained by Bertrand and Peelle [23]. All numerical data were retrieved from EXFOR library [17]. The calculation results are shown with solid lines and the experimental observations are shown with open circles.

For an incident proton energy of $E_p = 61.7$ MeV at 30° in the laboratory system, Fig. 3(a) compares the ^{209}Bi$(p,\ p'x)$ spectra calculated using the adjusted WKB solution [3] and

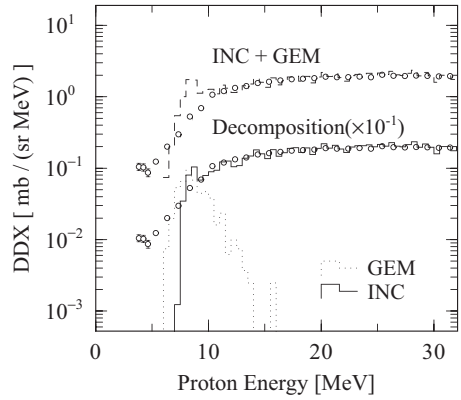

FIG. 11. ^{197}Au$(p, p'x)$ spectra at 50° for $E_p = 61.5$ MeV. Dashed line, sum of INC and GEM; solid line, INC component; dotted line, GEM component.

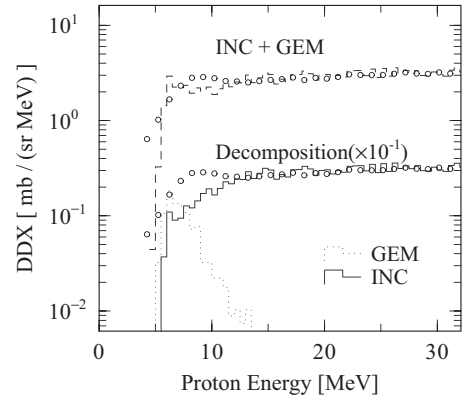

FIG. 12. ^{120}Sn$(p, p'x)$ spectra at 30° for $E_p = 61.5$ MeV. Dashed line, sum of INC and GEM; solid line, INC component; dotted line, GEM component.

the conventional method in which $P_{\rm tr}^{(p)}$ is unity above the threshold, and Fig. 3(b) compares the ^{209}Bi$(p, p'x)$ spectra calculated using the adjusted WKB solution and the present method. Below 20 MeV, the WKB-based spectrum agrees better with the experimental data than does that based on the conventional method. However, the WKB-based spectrum differs from the experimental data in three energy regions, namely, (i) the prominent bump at energies of 20–30 MeV, which was highlighted in Sec. I, (ii) the slight overestimation in the threshold region, and (iii) the difference above 55 MeV, which can be attributed to the treatment of low-energy collective excitation and beyond the scope of this study. By contrast, the present method reproduces the experimental spectrum very well: The bump disappears, and the overestimation in the evaporation region is improved. Note here that the present method includes no free parameters and provides the transmission coefficient with relatively low uncertainty.

In Fig. 4, the calculated ^{209}Bi$(p, p'x)$ spectra for $E_p =$ 61.7 MeV are compared with experimental spectra at angles of 30°, 60°, and 90°. The calculated spectrum reproduces the experimental spectrum at each angle.

In Fig. 5, the calculated ^{209}Bi$(p, p'x)$ spectra for $E_p =$ 38.7 MeV are compared with the experimental spectra at angles of 20–90°. The calculation results agree well with experimental data at every angle.

In Figs. 6 and 7, the calculated ^{197}Au$(p, p'x)$ spectra are compared with the experimental spectra at angles of 30–130° for $E_p = 61.5$ and 28.8 MeV, respectively. Similarly to the ^{209}Bi case, the calculated spectra for $E_p = 61.5$ MeV reproduce the experimental spectra without overestimation in the energy range of 20–30 MeV. For $E_p = 28.8$ MeV, reasonable agreements are obtained at 30–130°.

In Figs. 8 and 9, the calculated ^{120}Sn$(p, p'x)$ spectra are compared at angles of 30–125° for $E_p = 61.5$ MeV and 28.8 MeV, respectively. The calculation results for $E_p = 61.5$ MeV are in better agreement than those for the ^{209}Bi target. For $E_p = 28.8$ MeV, the calculated spectra reproduce the experimental spectra.

To discuss the evaporation region, the $(p, p'x)$ spectra for ^{209}Bi, ^{197}Au, and ^{120}Sn up to 30 MeV are shown in Figs. 10–12, respectively, in which the upper parts and the lower parts of the figures show the same experimental values, but the lower parts are shifted down by one order. The upper parts are the comparison with present calculations (the sum of INC and GEM), indicated by dashed lines, and the lower parts show the comparison with decompositions, namely each of INC (solid line) and GEM (dotted line). The experimental $(p, p'x)$ spectra for ^{209}Bi and ^{197}Au exhibit a different trend to that of the ^{120}Sn$(p, p'x)$ spectrum around 10 MeV: As the energy of the outgoing protons decrease, the former decrease whereas the latter increases slightly. The calculated spectra for ^{209}Bi and ^{197}Au reproduce the experimental spectra better without the GEM than do those with the GEM. However, the GEM contributes effectively to the calculated ^{120}Sn$(p, p'x)$ spectrum, but even with the GEM the calculation underestimates experimental data around 10 MeV.

IV. CONCLUSION

We developed a new method for determining the transmission coefficient for proton emission in $(p, p'x)$ reactions with no free parameters. In this method, we used empirical equations for the neutron-nucleus and proton-nucleus reaction cross sections as inverse processes. We applied the transmission coefficient to the INC calculation and compared the calculated $(p, p'x)$ spectra with experimental data for heavy target nuclei and an incident proton energy of around 50 MeV. The present results agreed better with the experimental spectra than did those based on a WKB solution. The evaporation contributions to the spectra for ^{209}Bi and ^{197}Au were not important.

[1] H. W. Bertini, Phys. Rev. **188**, 1711 (1969).
[2] J. Aichelin and H. Stocker, Phys. Lett. B **176**, 14 (1986).
[3] Y. Uozumi, T. Yamada, and M. Nakano, J. Nucl. Sci. Technol. **52**, 264 (2015).

[4] J. Cugnon, Few-Body Syst. **53**, 143 (2012).
[5] M. Kawai, Prog. Theor. Phys. **27**, 155 (1962).
[6] Y. L. Luo and M. Kawai, Phys. Rev. C **43**, 2367 (1991).
[7] Y. Uozumi, T. Yamada, S. Nogamine, and M. Nakano, Phys. Rev. C **86**, 034610 (2012).
[8] Y. Uozumi, Y. Yamaguchi, G. Watanabe, Y. Fukuda, R. Imamura, M. J. Kobra, and M. Nakano, Phys. Rev. C **97**, 034630 (2018).
[9] M. J. Kobra, G. Watanabe, Y. Yamaguchi, Y. Uozumi, and M. Nakano, J. Nucl. Sci. Technol. **55**, 209 (2018).
[10] A. Bubak, A. Budzanowski, D. Filges, F. Goldenbaum, A. Heczko, H. Hodde, L. Jarczyk, B. Kamys, M. Kistryn, S. Kistryn *et al.*, Phys. Rev. C **76**, 014618 (2007).
[11] J. R. Huizenga, A. N. Behkami, I. M. Govil, W. U. Schroder, and J. Toke, Phys. Rev. C **40**, 668 (1989).
[12] B. J. Fineman, K. T. Brinkmann, A. L. Caraley, N. Gan, W. J. Kernan, R. L. McGrath, and T. A. Savas, Phys. Rev. C **51**, 3184 (1995).
[13] B. Fornal, G. Prete, G. Nebbia, F. Trotti, G. Viesti, D. Fabris, K. Hagel, and J. B. Natowitz, Phys. Rev. C **37**, 2624 (1988).
[14] G. La Rana, R. Moro, A. Brondi, P. Cuzzocrea, A. D'Onofrio, E. Perillo, M. Romano, F. Terrasi, E. Vardaci, and H. Dumont, Phys. Rev. C **37**, 1920 (1988).
[15] G. Viesti, B. Fornal, D. Fabris, K. Hagel, J. B. Natowitz, G. Nebbia, G. Prete, and F. Trotti, Phys. Rev. C **38**, 2640 (1988).
[16] K. H. N. Murthy, S. K. Gupta, and A. Chatterjee, Z. Phys. A **305**, 73 (1982).
[17] EXFOR/CSISRS Experimental Nuclear Reaction Data [https://www.nndc.bnl.gov/exfor/exfor.htm].
[18] S. Pearlstein, Astrophys. J. **346**, 1049 (1989).
[19] K. Niita, H. Takada, S. Meigo, and Y. Ikeda, Nucl. Instrm. Meth. B **184**, 406 (2001).
[20] Q. B. Shen, INDC(CPR)-020, International Atomic Energy Agency, 1991 (unpublished).
[21] H. P. Wellisch and D. Axen, Phys. Rev. C **54**, 1329 (1996).
[22] S. Furihata and T. Nakamura, J. Nucl. Sci. Technol. **39**, 758 (2002).
[23] F. E. Bertrand and R. W. Peelle, Phys. Rev. C **8**, 1045 (1973).